

An Assessment of Short-medium Term ~~Intervention Effects~~ Interventions Using CAESAR-Lisflood in a Post-earthquake Mountainous Area

Di Wang^{1,2,3}, Ming Wang¹, Kai Liu¹, Jun Xie¹

¹School of National Safety and Emergency Management, Beijing Normal University, Beijing, China.

²Academy of Disaster Reduction and Emergency Management, Beijing Normal University, Beijing, China.

³Faculty of Geographical Science, Beijing Normal University, Beijing, China.

Correspondence to: Ming Wang (wangming@bnu.edu.cn)

Abstract. The 2008 Wenchuan earthquake rapidly triggered local geomorphic changes ~~rapidly, producing, shifting~~ abundant material through exogenic processes and creating vast amounts of loose material. The substantial material dynamics increased the risks of geo-hazards (flash floods, landslides, and debris flows) induced by extreme precipitation in the area. Intervention measures such as dams, levees, and vegetation revetments have been constructed in specified sites to reduce sediment transport, thus mitigating the risk of ensuing geo-hazards.

This study ~~focused on assessing intervention~~ assessed the effects of various interventions, incorporated with ~~various multiple~~ facilities, on post-earthquake fragile mountains in the short-medium term. Taking the Xingping valley as an example, we used ~~the~~ CAESAR-Lisflood software, a two-dimensional landscape evolution model, to simulate three scenarios: unprotected landscapes, present protected landscapes, and enhanced protected landscapes between 2011 and 2013. We defined two indicators to assess the intervention effects of the three scenarios by comparing the geomorphic changes and sediment ~~yield-~~ yields. The results ~~showed~~ show that the mitigation facilities ~~were~~ are effective, especially engineering efforts cooperating with vegetation revetments in the upstream area. The spatial patterns of erosion and deposition ~~changed~~ change considerably ~~caused~~ due to the intervention measures. Additionally, the effectiveness of each intervention scenario ~~showed~~ shows a gradual decline over time caused directly by the reduction ~~of~~ in the reservoir's capacity. The enhanced scenario ~~functioned~~ performs better than the present one, with a smaller downward trend. The simulation results ~~assessed~~ assess the ability and effectiveness of cooperated control measures and ~~could~~ will support optimum mitigation strategies.

1 Introduction

Strong earthquakes can trigger co-seismic landslides ~~and crack the mountains~~, discontinuously, increasing crack mountains, and thus increase weak structural planes (Huang, 2009) by weathering and erosion. Consequently, ~~the source~~ material ~~produced~~ shifted from ~~co-seismic~~ co-seismic landslides and attendant mass ~~failure~~ failures caused by ~~the weak slope increase in~~ mountainous regions and weakened slopes modify mountain landscapes by various surface processes for days, years, and millennia (Fan et al., 2020). The 2008 Wenchuan Ms 8.0 (the surface-wave magnitude, which is the logarithm of the maximum amplitude of the ground motion ~~for~~ of the surface waves with a wave period of 20 seconds) earthquake has been influencing towns and other infrastructure in the affected area. Many studies have mapped the landslides triggered by ~~the~~ this devastating earthquake. One study, Gorum et al. (2011), performed an extensive landslide interpretation using a large set of high-resolution optical images and mapped nearly ~~60000~~ 60,000 individual landslides, which are no less than all impacting an area of 600 m² or more. Another study, Xu et al. (2014), delineated ~~197481~~ 197,481 landslides formed by polygons, centroids, and top points compiled from visual image interpretation. To estimate the threat of loose material in subsequent sediment disasters caused by landslides, some research ~~attempt~~ has attempted to measure the volume of deposited material based on field ~~surveys~~ surveys and

38 assumptions. ~~For example,~~ Huang and Fan (2013) estimated ~~that~~ 400 million m³ of material ~~was~~ deposited in ~~the heavy-heavily~~
39 affected areas by assuming that the material ~~was~~ deposited on steep slopes with angles larger than 30° and a catchment area of
40 more than 0.1 km². An approximate ~~27932,793~~ million m³ of sediment was calculated by Chen et al. (2009) using different
41 deposited depth settings in different buffer zones of the Longmenshan central fault. In summary, a tremendous ~~number~~~~amount~~
42 of loose material accumulated ~~on~~~~in~~ the gullies and hillslopes, ~~ready to be eroded~~ ~~which became available for erosion~~ and
43 ~~transported away over a long time~~~~other exogenic processes for years to come~~. As a result, ~~the~~ mitigation in the Wenchuan
44 ~~quake~~~~earthquake~~-stricken area is still ~~in the long run~~~~ongoing~~.

45 Structural mitigation measures have been developed in the affected areas ~~regarding~~~~depending on~~ the ~~different~~ site conditions
46 and ~~other~~ technical and economic feasibilities. For example, ecological mitigation, such as vegetation revetments, was con-
47 ducted to stabilise the source area in hillslopes (Cui and Lin, 2013; Forbes and Broadhead, 2013; Stokes et al., 2014), and
48 check dams were used widely to intercept upriver sediment (Yang et al., 2021; Marchi et al., 2019). ~~Lateral~~~~And lateral~~ walls
49 and levees ~~were the longitudinal~~~~which are longitudinal~~ structures (Marchi et al., 2019), ~~can be built~~ to protect ~~the infrastructure~~
50 ~~sinfrastructure~~ in mountain watersheds with ~~relatively~~ higher sediment ~~supply to the~~~~runoff into~~ main streams.

51 Although comprehensive mitigation measures were performed ~~in~~~~at~~ potentially dangerous sites, disasters still occurred ~~owing~~
52 ~~due~~ to rough terrain, vague source material, intensive precipitation, and relatively low-cost ~~mitigating~~~~mitigation~~ measures (Yu
53 et al., 2010; Cui et al., 2013). Therefore, understanding the effectiveness of intervention measures is crucial for mitigation
54 strategies. Some studies ~~mainly~~ focus on establishing post-evaluation effectiveness index systems that are not supported by
55 sufficient practices (Zhang and Liang, 2005; Wang et al., 2015). Some researchers compare the changes before and after ~~the~~
56 intervention measures ~~recorded~~ by ~~the~~~~recording~~ long-term on-site ~~measurement~~~~measurements~~, which face the challenges ~~to~~
57 ~~the investment~~ of ~~much~~~~needing a great deal of~~ time, energy and financing (Zhou et al., 2012; Chen et al., 2013). Recent research
58 ~~compares the~~~~has compared~~ disaster characteristics before and after ~~the~~ mitigation actions, which are quickly obtained from ~~the~~
59 numerical ~~simulations~~~~simulations~~ (Cong et al., 2019; He et al., 2022). Nevertheless, these disaster characteristics ~~express the~~
60 ~~process ignoring~~~~ignore~~ the long-~~time~~~~term~~ effects ~~of earthquakes~~ on ~~the~~ geomorphic changes (longer than the duration of a
61 single event). Therefore, the short-medium term (from the duration ~~of a single event~~ to decades ~~after~~) and spatial geomorphic
62 changes ~~quickly~~ obtained from ~~the simulation will~~~~simulations~~ provide more details to interpret engineering measures in notable
63 locations, even in ~~these~~~~locations~~ inaccessible to humans.

64 CAESAR-Lisflood (C-L), which is based on the ~~Cellular Automata~~~~cellular automata~~ (CA) framework (Coulthard et al., 2013),
65 has powerful spatial modelling and computing capabilities to simulate complex dynamic systems (Batty and Xie, 1997; Cou-
66 clelis, 1997; Coulthard et al., 2002). The model enables the study of many earth system interactions under different geo-
67 environmental. Representation of deposition and erosion within C-L is used widely in rehabilitation planning and soil erosion
68 predictions ~~from a~~~~in~~ post-mining ~~landform~~~~landforms~~ (Saynor et al., 2019; Hancock et al., 2017; J.B.C. Lowry et al., 2019;
69 Thomson and Chandler, 2019; Slingerland et al., 2019) ~~and as well as~~ channel evolution and sedimentary budget ~~with~~~~planning~~
70 ~~for~~ dam settings (Poepl et al., 2019; Gioia and Schiattarella, 2020; Ramirez et al., 2020, 2022). In addition, there ~~were~~~~have~~
71 ~~been~~ a series of studies ~~in the~~ mountainous area involving secondary geo-hazard driving factors (Li et al., 2018; Wang et al.,
72 2014b) and vegetation recovery (Zhang et al., 2018). ~~One study,~~ Li et al. (2020) and Xie et al. (2018) ~~have~~ used C-L with
73 different rainfall ~~scenarios or and~~ future climate change ~~scenarios~~ to interpret the landscape evolution after the Wenchuan earth-
74 quake. The methods and parameter values used in the above research helped ~~to~~ promote ~~the~~~~this model's~~ application in other
75 study areas.

76 In this study, ~~the~~ hourly rainfall data ~~of over~~ three years ~~was~~~~were~~ generated by ~~daily~~ downscaling ~~from daily~~ to capture ~~the~~
77 extreme ~~event~~~~events~~. Based on the input data, we simulated and compared the geomorphic changes and sediment yield in three
78 scenarios that varied in ~~their~~ mitigation compositions and intensities in ~~at the~~ catchment. The objectives ~~are~~~~were~~ 1) to 1) assess

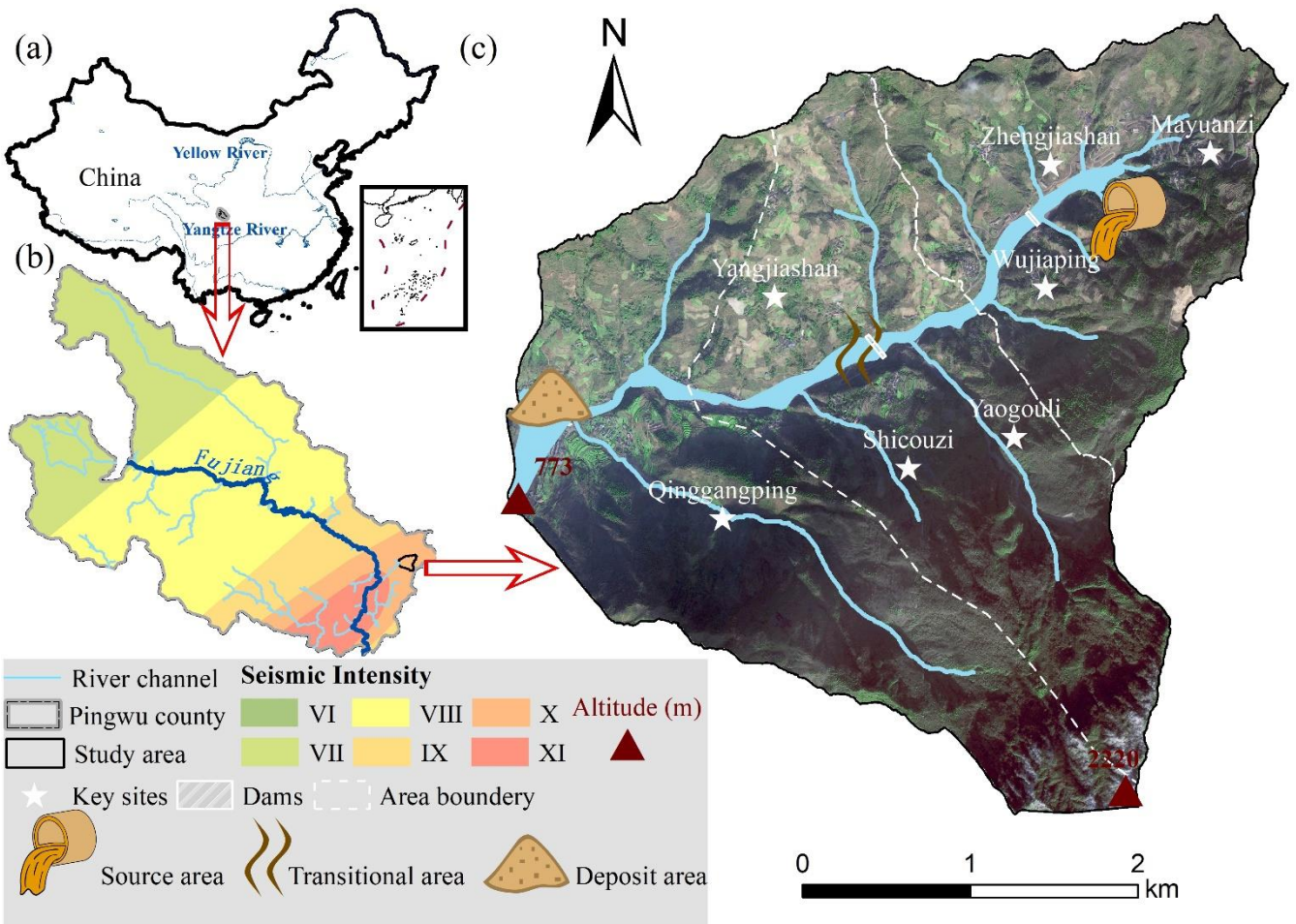
79 the effectiveness of a set of mitigation facilities to reduce sediment transport, 2) to analyse the role of each facility on geo-
 80 morphic changes, and 3) to determine the influence of vegetation-influence on catchment erosion.

81 **2 Study area**

82 **2.1 Regional characteristics**

83 The study area was the Xingping valley in the northeastern north-eastern Sichuan province, a Province, the left branch of the
 84 Shikan riverRiver (a tributary of the Fu River) (Fig. 1)(Fig. 1). There are nearly two hundred households scattered among
 85 more than five villages in the catchment. The topography of the catchment is rugged, with an elevation between 800 and 3036
 86 m and an area of approximately 14 km². The catchment is characterised by a high longitudinal gradient (~ 120‰) and more
 87 than ten small V-shaped branch gullies. The length from the northeast to the southwest is 57705.770 m, and the other direc-
 88 tionwidth is 4,150 m in the perpendicular to which is 4150 m. A direction. The region has a humid temperate climate with a
 89 mean annual temperature of 14.7°C characterises the region. The mean annual precipitation is 807.6 mm, mainly concentrated
 90 between May and September. The steep terrain and short-term heavy rainfall make andominate ephemeral streamstreams in
 91 this area.

92 The local basement rocks are mainly metamorphic sandstones, sandy slate, crystalline limestone, and phyllite of the Triassic
 93 Xikang Group (T_{3xk}) and Silurian Maoxian Group (S_{mx}), which are easily worn away by quicklyquick weathering in a static
 94 processprocesses after disturbed in a disturbs caused from strong earthquakeearthquakes. Consequently, the Wenchuan earth-
 95 quake, with a Modified Mercalli Intensity scale of X, made this area one of the most severely affected locations (Wang et al.,
 96 2014a) and produced 10⁶ m³ loose material by triggering landslides and subsequent weathering in Mayuanzi, Zhengjiashan,
 97 and Wujiaping (Fig. 1)(Guo et al., 2018)(Fig. 1)(Guo et al., 2018).



99 **Figure 1: Overview** An overview of the study area. (a) **Location** The location of the study area; (b) **Seismic** A seismic intensity map of
100 the Wenchuan earthquake within the Pingwu county; (c) **The** A schematic image of the study area.

101 2.2 Historical hazards and intervention measures

102 Six ~~group~~ debris flow-flash flood disaster ~~chains~~ chain groups have been found in the Xingping valley over ~~a~~ the decade after
103 the earthquake. Based on the published work of SKLGP (State Key Laboratory of Geohazard Prevention and Geoenvironment
104 Protection) and the local states' geological survey before 2018 and our biannual field surveys since 2012, we catalogued the
105 time of occurrence, total rainfall of each event, and corresponding disaster details (Table S1). The massive sediment was
106 transported quickly after the devastating ~~quake~~ earthquake in 2008 and 2009, and the extreme rainfall in 2013 and 2018 trig-
107 gered ~~prosperous~~ the deposition of extensive loose material ~~deposited~~ in the channel. Considering the landslide processes, we
108 divided the study area into three regions: the source area, the transitional area, and the deposit area (~~the~~ The white dashed
109 lines in Fig. 1c), which means Fig. 1c indicate that the loose solid material ~~would be can~~ easily ~~be~~ transported from the source
110 area to the deposit ~~one~~ area through the transitional zone.

111 An engineering control project was constructed to intercept the upriver material in October 2010. The project included two
112 check dams, one in the upper source area and the other in the transitional zone (Feng et al., 2017) (~~Fig. 1e~~(Fig. 1c). The upper
113 dam has a storage capacity of 5.78×10^4 m³ and a height of 10.0 m. The transitional area dam has a storage capacity of 7.2×10^4
114 m³ and a height of 9.0 m. With the reservoirs gradually filling with deposits, the first dredging work was subsequently ~~done~~
115 ~~performed~~ in 2013. Nearly three years later, the storage capacity behind the upper dam remained at 50% in 2016, while the
116 transitional area dam ~~can~~ could no longer retain sediment.

117 3 Materials and Methods

118 In this study, we examined the intervention effectiveness through the morphological response and sediment yield in the Xing-
119 ping valley, which was simulated using the C-L model. The research entailed four main steps: 1) setting three scenarios with
120 different intervention compositions, 2) preprocessing the model input data, including three groups of DEMs, the rainfall data,
121 and the m value of the C-L, 3) calibration of the hydrological component, and 4) simulating landscape changes and analysing
122 the intervention effectiveness in 2011-2013.

123 3.1 Scenarios Scenario settings

124 The abundant source material triggered by landslides should be controlled to prevent the threat of disasters downstream. There-
125 fore, we designed three scenarios by incorporating engineering and biological measures referenced to current facilities to assess
126 the effectiveness of intervention measures. Scenario UP: Unprotected landscapes meant the ~~sediments~~ sediment would
127 ~~transport~~ be transported without anthropogenic intervention. Scenario PP: Present protected landscapes implied that only the
128 present two check dams trapped ~~deposits~~ sediment in 2011-2013 without dredging work over the period (see ~~section~~ Section
129 2.2). Scenario EP: Enhanced protected landscapes emphasised the ~~plus~~ addition of vegetation revetments in the source area and
130 levees in the deposit area based on the two check dams in Scenario PP.

131 ~~Fig. 1e~~ Figure 1c shows the locations of the existing two check dams in both Scenario PP and Scenario EP. We determined the
132 placements of additional facilities in Scenario EP according to the field survey, which demonstrated that the continuous supply
133 of ~~sediments~~ sediment was mainly from the source area. Therefore, ~~the~~ vegetation revetments ~~like~~ such as tree planting would
134 be carried out ~~in~~ upstream to prevent erosion by stabilising the topsoil and enhancing the soil's infiltration capacity ~~with its~~ via
135 roots (Lan et al., 2020).

136 Considering the ~~damages~~ damage caused by flash ~~flood~~ floods to the residential area downstream, the levees (see Fig. S1 and
137 Section 3.2.2) are artificial barriers to protect agricultural land and buildings, which ~~helped~~ help to prevent water and sediment

138 from overflowing and flooding surrounding areas. Table 1 shows the scenario descriptions, initial model conditions and input
 139 rainfall series. The details about [the](#) model input data are introduced below.

140 **Table 1: ~~Scenarios setting~~Scenario settings**

Scenario	Descriptions	Period	DEM (10m 10 m)	Rainfall data
UP	no anthropogenic intervention		UP DEM	downscaled hourly pre- cipitation is over the pe- riod
PP	the present two check dams upstream without dredging work	2011-2013 (3 years)	PP DEM PP bedDEM	(lumped) downscaled hourly pre- cipitation is over the pe- riod
EP	additional vegetation revetments in the source area and levees in the deposit area based on Scenario PP		EP DEM EP bedDEM	(spilt)

142 3.2 CAESAR-Lisflood

143 The C-L integrated the Lisflood-FP 2D hydrodynamic flow model (Bates et al., 2010) with the CAESAR landscape evolution
 144 model (LEM) (Coulthard et al., 2002; Van De Wiel et al., 2007), which is described in detail by Coulthard et al. (2013). The
 145 catchment mode of C-L was applied in this study, [withinin](#) which the surface digital elevation model (DEM), the bedrock DEM,
 146 the grain size distribution, and a rainfall time series are required to simulate the sediment transport and geomorphic changes.

147 There are four primary modules within C-L operated as follows:

- 148 (1) a hydrological module generates surface runoff from rainfall input using an [adaptionadaptation](#) of TOPMODEL ([Topogra-
phy-topography](#)-based hydrological model) (Beven and Kirkby, 1979),
- 149 (2) a hydrodynamic flow routing module based on the Lisflood-FP method (Bates et al., 2010) [which](#) calculates the flow depths
 150 and velocities,
- 151 (3) an erosion and deposition module uses hydrodynamic results to drive fluvial erosion by either the Einstein (1950) or the
 152 Wilcock et al. (2003) [equationequations](#) applied to each sediment fraction over nine different grain sizes,
- 153 (4) and a slope model [movesof the movement of](#) material from the hillslope to the fluvial system by considering both the mass
 154 movement when a critical slope threshold is exceeded; and soil creep processes whereby sediment flux is linearly proportional
 155 to [the](#) surface slope.

156 The C-L model updates variable values stored in square grid cells at intervals, such as DEM, grain size and proportion data,
 157 water depth, and velocity. For [the](#) three scenarios, the initial conditions, such as DEMs and bedrock DEMs, the rainfall data,
 158 and the m values, were preprocessed as follows.

160 3.2.1 ~~Surface~~[The surface](#) and bedrock digital elevation ~~model-models~~

161 To [clearly](#) describe ~~clearly~~ the control process, especially the two dams and levees in the catchment, we unified grid cell scales
 162 to 10 m for all input data of the C-L. The GlobalDEM product with a 10 m × 10 m resolution and 5 m (absolute) vertical
 163 accuracy ~~was were~~ used to form three types of initial DEMs (UP DEM, PP DEM, and EP DEM). Before rebuilding [the](#) initial
 164 DEMs, we filled the sinks of the original GlobalDEM based on [the](#) Environmental Systems Research Institute's (ESRI's)
 165 ArcMap (ArcGIS, 10.8) to eliminate the 'walls' and the 'depressions' in the cells and [thus](#) avoided ~~the~~ intense erosion or depo-
 166 sition in the early run time. Then, the non-~~sinks~~sink DEM was used as the surface DEM in Scenario UP (UP DEM) without
 167 any facilities. According to the engineering control project described in Section 3.2.2, [the](#) surface DEM of Scenario PP (PP
 168 DEM) included the dams by raising the grid cell elevations by 10 m for the dam in [the](#) upper stream and 9 m for the dam in
 169 the transitional area. Similarly, the surface DEM in Scenario EP (EP DEM) included the dams in [the](#) PP DEM. In addition, two

170 levees were produced by raising the grid cells' cell elevation by 2 m that were represented, representing at selected locations.
171 For scenario EP, the placement and setting of the vegetation revetments in Scenario EP were introduced in Section 3.2.2.
172 The spatial heterogeneity of the source material (Fig. 1e(Fig. 1c)) indicates the discrepancy of the erodible thickness, which
173 equals the difference between the surface DEM (DEM) and the bedrock DEM (bedDEM). We divided the study area into five
174 regions according to the erodible thickness (Fig. S1) by checking out the relative elevation of the foundations of buildings, the
175 exposed bedrock, and the deposited deposition depth of landslides to the ground level. The average thicknesses of upstream
176 low- and high-altitude areas were set to 10 m and 3 m, respectively, and the thickness of the erodible layer in the downstream
177 area was set to 3 m. For the river channel and outlet, as there would be a large amount of deposition, the thickness of erodible
178 sediment was set to 5 m and 4 m, respectively. As the dams in Scenario PP and the levees in Scenario EP were non-erosive
179 concrete, we set the erodible thickness of these features to 0 m. Eventually, DEMs the DEM data were formatted to ASCII
180 raster data as required by C-L. The divided regions varied in erodible thickness, the placement of additional levees and vege-
181 table revetments in Scenario EP, and the generation process of DEMs and bedDEMs were shown in Fig. S1.

182 3.2.2 Vegetation settings

183 Another parameter required in each scenario simulation was the m value of the hydrological model (TOPMODEL) within C-
184 L, which controls the exponential decline of transmissivity with depth (Beven, 1995, 1997) and influences the peak and
185 duration of the hydrograph in response to rainfall. The m value effectively imitates the effect of vegetation on the movement
186 and storage of water within the soil. The lower the m value is, the lower the vegetation coverage, and the flashier higher the
187 flash flood peak and the shorter the duration are reflected in of the flood hydrograph is reflected (Coulthard et al., 2002). The
188 m value is usually determined by the land cover (e.g., 0.02 for the forest, forests and 0.005 for the grassland grasslands)
189 (Coulthard and Wiel, Van De J., 2017). In our study, we set the m value as 0.008 in our smaller catchment (14 km²) in Scenario
190 UP and PP, which resembles the m value of farmland covered with lower vegetation coverage in the same catch-
191 ment studied by Xie et al. (2018) and Li et al. (2018). As mentioned earlier, the upstream-low elevation area covered by the
192 biological measures in the EP scenario was assigned a higher m value of 0.02. This m value was calibrated by the
193 more extensive catchment containing our study area by replicating in the flood event in of 2013 (Xie et al., 2018).

194 3.2.3 Rainfall The rainfall data

195 In this research, we compared three scenarios with identical by matching precipitation data between 2011 and 2013, as men-
196 tioned in Section 3.1. The source data of precipitation in 2011-2013 (Fig. 2a) was (Fig. 2a) were obtained from the China
197 Meteorological Administration (<http://data.cma.cn>) (<http://data.cma.cn>) with daily temporal resolution. The intensity and fre-
198 quency of extreme rainfall events affect patterns of erosion and deposition (Coulthard et al., 2012b; Coulthard and Skinner,
199 2016). Therefore, we used the stochastic downscaling method to generate hourly data to better capture the hydrological events
200 introduced by Li et al. (2020) and Lee and Jeong (2014). The referenced hourly precipitation was observed from the pluviom-
201 eter located 20 km from the study area in 2016 (Fig. 2b(Fig. 2b)), with an annual total precipitation of 684 mm. The observed
202 rainfall in 2016 was characterised by: (1) hourly precipitation was from between 1.1 mm to and 35.4 mm; and (2) the maximum
203 and average duration durations of a rainfall event were as 24 h and 2.8 h, respectively. The main processes of the downscal-
204 ing method are as follows:

- 205 ● extracting the hourly rainfall of specific days in 2016 closest to the daily rainfall in 2011-2013 through the threshold
206 setting and producing the genetic operators using the extracted hourly rainfall dataset;
- 207 ● mixing the genetic operators by genetic algorithm (Goldberg, 1989) composed of reproduction, crossover and mu-
208 tation and repeating until the distance between the sum of hourly rainfall and the actual daily rainfall is less than the
209 set threshold;

● normalising the hourly precipitation to ~~remain~~keep the daily rainfall value unchanged.

Figure 2c shows the downscaled rainfall series between 2011 and 2013. The downscaled hourly rainfall better captured the hydrological events at an hourly scale compared to the hourly-mean rain (5.27 mm) on the day with extreme rainfall (126.5 mm), which was far from the actual situation. Corresponding to the m value settings, the input of generated hourly precipitation ~~is~~was catchment lumped in Scenario UP and Scenario PP and divided into two separate but identical rainfall ~~events~~ in Scenario EP.

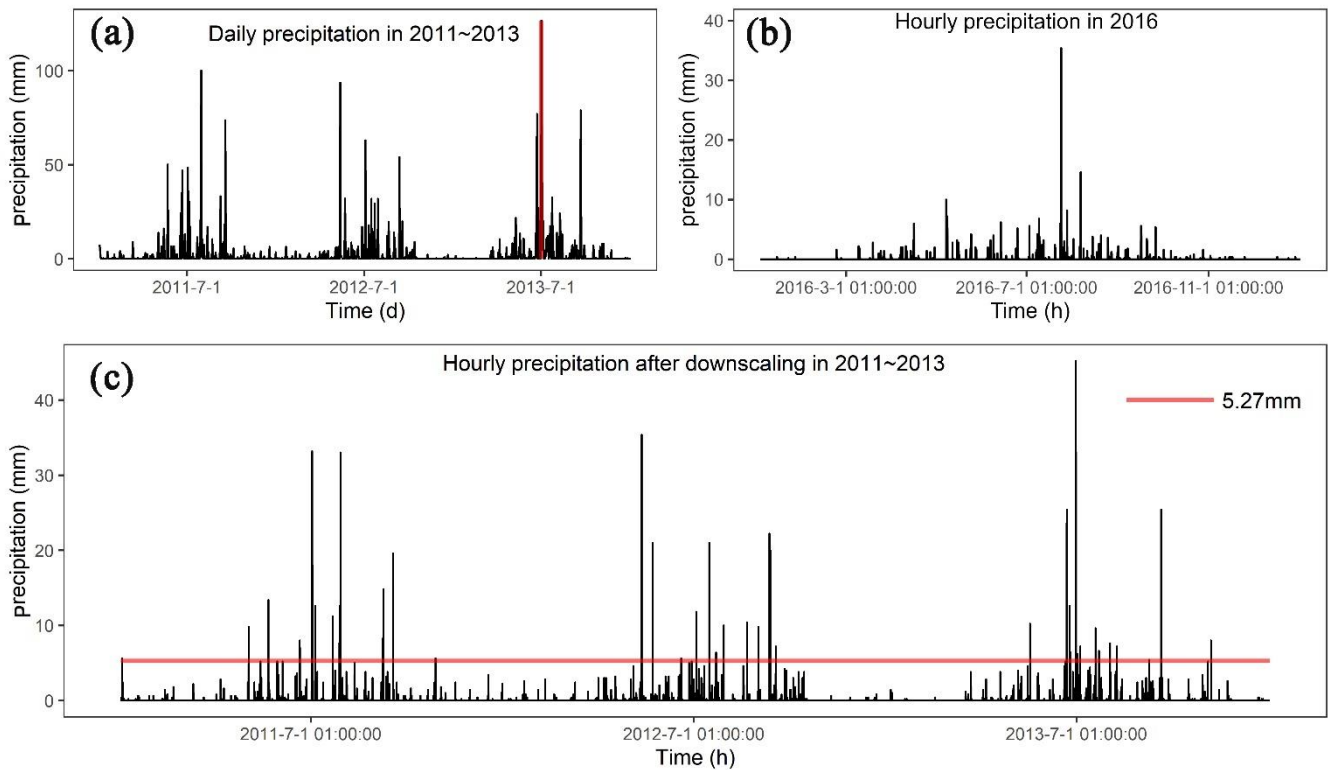


Figure 2: (a) Daily precipitation in 2011-2013 (the red vertical line indicates the maximum daily precipitation of 126.5 mm); (b) Hourly precipitation in 2016; (c) Downscaled hourly precipitation in 2011-2013 (the red horizontal line indicates the hourly-mean precipitation of 5.27 mm on the day with the maximum precipitation marked in (a)).

3.2.4 Other parameters

The C-L model is sensitive to a set of input data introduced by Skinner et al. (2018) for a catchment with a grid cell size of 10 m, such as the sediment transport formula, slope failure threshold, and grain size set. The grain size distribution of sediment ~~is~~was derived from samplings at 14 representative locations in the same study basin by Xie et al. (2018). Given the grain size distribution in this study, the Wilcock and Crowe formula was selected as the sediment transport rule, which was developed from flume experiments using five different sand-gravel mixtures with grain sizes ranging between 0.5 and 64 mm (Wilcock et al., 2003). Considering the steep slopes on both sides of deep gullies, a higher slope failure threshold was determined to replicate the geomorphic changes between 2011 and 2013. Additionally, we found that the probability of shallow landslides indeed accumulated and increased from 20° to 50° in slope gradient between 2011 and 2013 (Li et al., 2018). The slope angle was derived from the DEM with a 30 m spatial resolution, which caused a lower slope angle than that with a 10 m resolution. As such, we set the slope angle as 60°, which is lower than the 65° used in a scenario without landslides (Xie et al., 2022) and higher than 50°. Some parameters were determined by repeated experiments, such as the minimum Q value, and the other input values were referred to default values recommended by the developers (such as the maximum erosion limit in the erosion/deposition module and the vegetation critical shear stress) in <https://sourceforge.net/p/caesar-lisflood/wiki/Home/>. Table S2 in the supplemental material presents the model parameters of C-L used in this study.

236 **3.2.5 Model calibration**

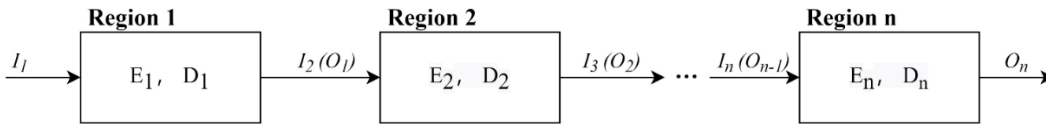
237 Considering the ungauged basins before 2015, we replicated the flash flood event in July 2018 using C-L simulations to cali-
 238 brate the hydrological components. Based on Scenario PP (with two checking dams), we ~~input~~used the two-week hourly pre-
 239 cipitation ~~in~~of July 2018 as the input (Fig. S2a), which ~~is~~was recorded by ~~the~~a rain gauge located 2.5 km away from the
 240 catchment (Fig. S2b). The simulation results (Fig. S2c and Fig. S2d) ~~show~~showed an erosion map and a maximum water
 241 depth map in Scenario PP on July 15, 2018. We selected three locations to compare the deposition and inundation in the
 242 simulation results, with satellite images and photos (Fig. S3). Additionally, the simulated sediment thickness and water depth
 243 were close to those measured from pictures, which indicated that the flash flood event was well replicated by the C-L using
 244 the input data.

245 **3.3 Output analysis**

246 The C-L model outputs ~~in~~of each scenario include hourly water and sediment discharge at the basin outlet, and the difference
 247 between DEMs at a specified time and initial DEMs (EleDiffs). We validated the model outputs by comparing the hourly
 248 discharge and EleDiffs reflecting the depth of sediment deposition or erosion (> 0.1 m: deposition, < -0.1 m: erosion) with
 249 field survey materials. The overall temporal and spatial geomorphic changes reflected by EleDiffs under three different sce-
 250 narios were used to assess the geomorphic response to interventions. To explore the geomorphic response to various control
 251 measures, we focused on the ~~key spots placed notable sites where the~~ checking dams, levees, and vegetation revetments would
 252 be located and recorded the depth of ~~deposited~~accumulating sediment behind the two dams. To further explore the spatial
 253 heterogeneity, we compared the volumes of deposition and erosion among three divided regions, including the source area, the
 254 transitional area, and ~~deposition~~the deposit area.

255 Based on the visual analysis and quantitative results, we defined two formulae to assess the effectiveness of the intervention.
 256 The conservation ability (Ca , Eq. (3)) was calculated based on variables in the sediment balance system (~~Fig. 3~~)(Fig. 3). The
 257 sediment volume of deposited sediment (D_n) and input sediment from the upper connected region (I_n) is equal to that of the
 258 eroded material (E_n) and the output sediment to the next part (O_n) over the same period (Eq. (1), Eq. (2)) in the system. A
 259 higher value of Ca in a specific region and scenario indicates ~~that~~a more effective control system ~~is~~applied.

260



261

262 **Figure 3: The sediment balance system in the study area (the Region n ~~indicated~~indicates the source area, transitional area, and**
 263 **deposit area)**

264

$$I_n = \sum_2^n E_{n-1} - \sum_2^n D_{n-1}, \quad (1)$$

$$I_n + E_n = O_n + D_n, \quad (2)$$

$$Ca = \frac{D_n}{I_n + E_n} \quad (3)$$

265 ~~Where, where~~ n is the region number of the source area (=1), transitional area (=2), and deposit area (=3).

266 Additionally, we designed the relative efficiency (Re , Eq. (4)) to depict the efficiency of intervention measures in Scenario PP
 267 and EP in sediment loss, with the comparison to Scenario UP.

$$Re_{PP/EP,i} = \frac{Q_{UP,i} - Q_{PP/EP,i}}{Q_{UP,i}} \quad (4)$$

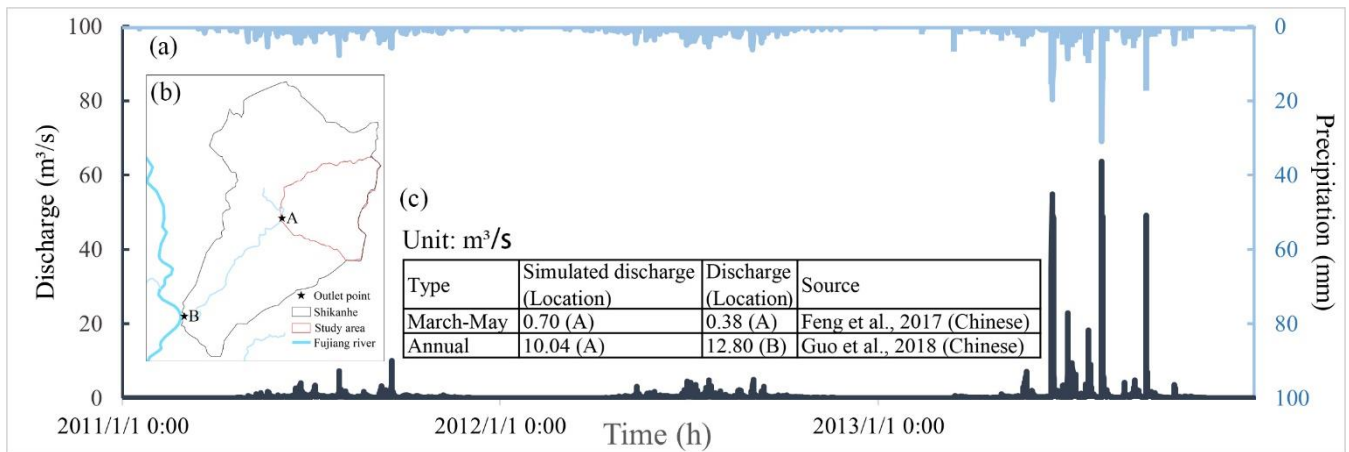
268 Where i is the sequence of the day; Q_{UP} is the daily sediment yield measured at the catchment outlet in Scenario UP;
 269 and $Q_{PP/EP}$ is the daily sediment yield measured at the catchment outlets same data in Scenario PP or Scenario EP of day i ; and
 270 $Re_{PP/EP}$ is the daily relative effectiveness of control measures in Scenario PP or Scenario EP.

271 4. Results

272 4.1 Model verification

273 Fig. 4 Figure 4 shows the input rainfall data and modelled discharge hydrograph between 2011 and 2013 (Fig. 4a(Fig. 4a)). The
 274 comparison of simulated mean discharge in April through July and the whole year with field survey materials in the
 275 locations are also presented (Fig. 4b(Fig. 4b, c)). Concerning the discharge hydrograph, the peak discharges (63.7, 54.9, and
 276 $50.3 \text{ m}^3/\text{s}$) correspond well with the peak rainfall intensities (31, 19.7 and 15 mm). The modelled water discharge from March
 277 to May in location A is slightly larger than the measured value reported by Feng et al. (2017). Additionally, an average annual
 278 discharge of $10.04 \text{ m}^3/\text{s}$ in location A is less lower than that of $12.80 \text{ m}^3/\text{s}$ in the catchment outlet (location B), which has an
 279 area approximately three times the size of the study area.

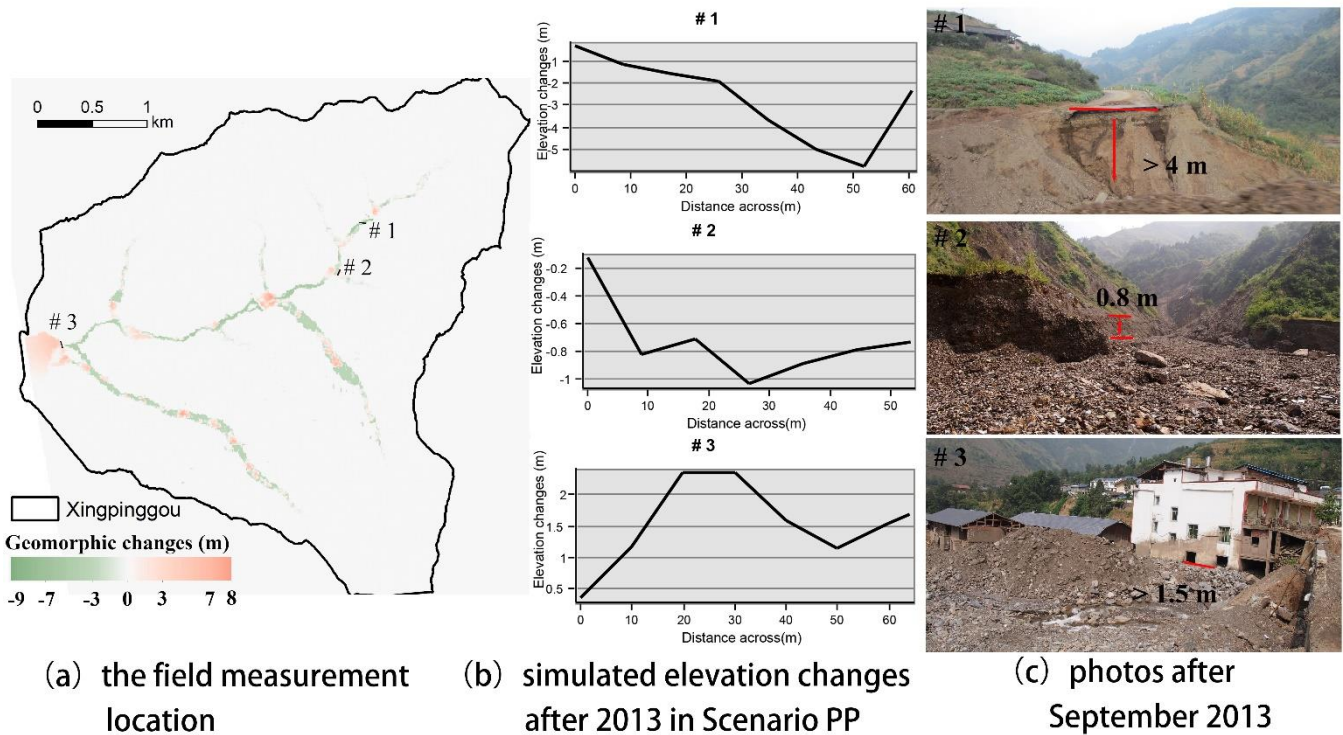
280



281

282 **Figure 4: The input and output of the hydrograph. (a) The input hourly precipitation and simulated discharge in 2011-2013 in**
 283 **Scenario PP; (b) LocationThe locations of the specified outlet pointpoints; (c) theA comparison of the simulated average discharge**
 284 **to the recorded discharge.**

285 Typical cross-sections are generated (Fig. 5(Fig. 5)) based on the replicated landscape changes in Scenario PP. The first site is
 286 located on the upriver road, which was is eroded at a depth of 5.7 m according to the simulation results, while the photo shows
 287 a depth of no less than 4.0 m without an apparent eroded base. The cross-section #2 and the site photo of the gully depict that
 288 the eroded depth is approximately 1.0 m. Meanwhile, a clear sediment boundary is found in the building located at the depos-
 289 ited area (# 3), indicating a slightly lower deposition depth than the modelled one-model predicted.



291

292

Figure 5: The comparison of cross-sections from the simulation results to the field measurements after 2013 in Scenario PP.

293

4.2 Overall geomorphic changes

294

295

296

297

298

299

300

301

302

303

304

305

306

307

308

309

310

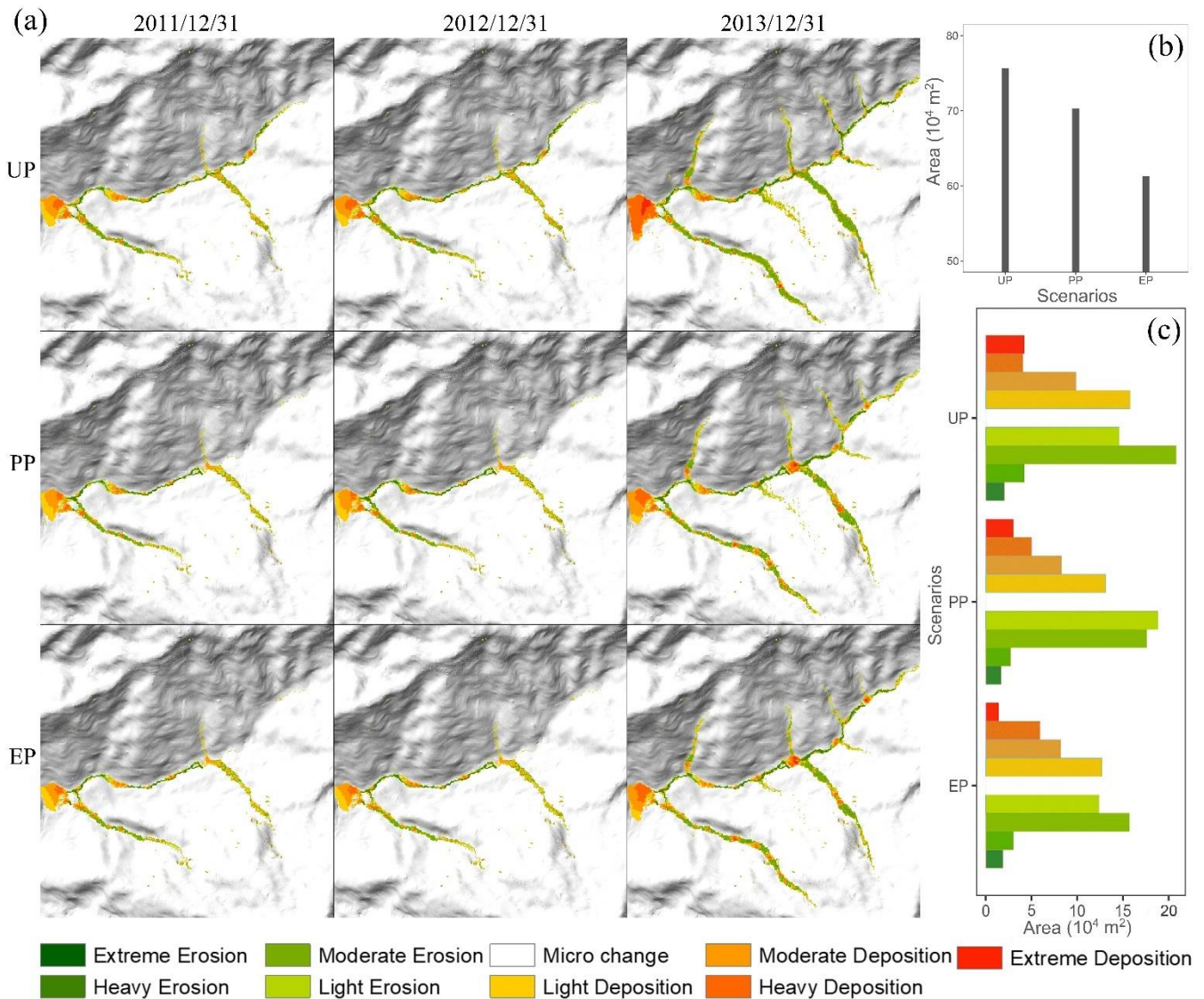
311

312

Figure 6a compares the three annual landscape changes in each scenario, which were classified into nine categories by natural breaks for EleDiffs: extreme erosion (< -7 m), heavy erosion (-7 to -3 m), moderate erosion (-3 to -1 m), light erosion (-1 to -0.1 m), micro change (-0.1 to 0.1 m), light deposition (0.1 to 1 m), moderate deposition (1 to 3 m), heavy deposition (3 to 7 m), and extreme deposition (> 7 m). A similar spatial pattern of erosion is observed in all three scenarios. More specifically, erosion mainly occurred in the main channel and the branch valleys, among which the left branches were more severe. In contrast, the deposition distribution appeared to be varied in the three scenarios, especially in the area behind the two dams shown in Scenario PP and EP.

The total area of affected grid cells representing erosion and deposition in each scenario was calculated to compare the difference (Fig. 6b). The affected area in Scenario UP was the largest at approximately 0.76 km² (5.4% of the total catchment), which was larger than that in Scenario PP (0.70 km², 5.0% of the whole catchment), and the affected area decreased to 0.61 km² (4.4% of the total catchment) in Scenario EP. The total area of erosion and deposition reduced gradually with more controlling measures established in this study.

Figure 6c compares the extent of geomorphic changes in three situations using the areas that varied in depth. The erosion area of the light and moderate erosion areas was more extensive than the extreme and heavy erosion areas for all three scenarios. The size of each erosion degree in UP was more extensive than that in PP and EP. In addition, the greater the deposition depth is, the smaller the deposition coverage. Especially, the extreme deposition area was somewhat more extensive than the area of the heavy deposition in the UP scenario. Further analysis shows that extreme, moderate, and light deposition areas decreased in the order of UP, PP, and EP. The heavy deposition areas show the opposite trend, mainly attributed to the checking dams and vegetation revetments.



314

315

316

Figure 6: (a) Simulated geomorphic changes over time for the three scenarios; (b) the affected area of deposition and erosion for the three scenarios; (c) The columnar distribution of different erosion and deposition levels.

317

4.3 Details of key spots locations

318

319

320

321

322

323

324

325

326

327

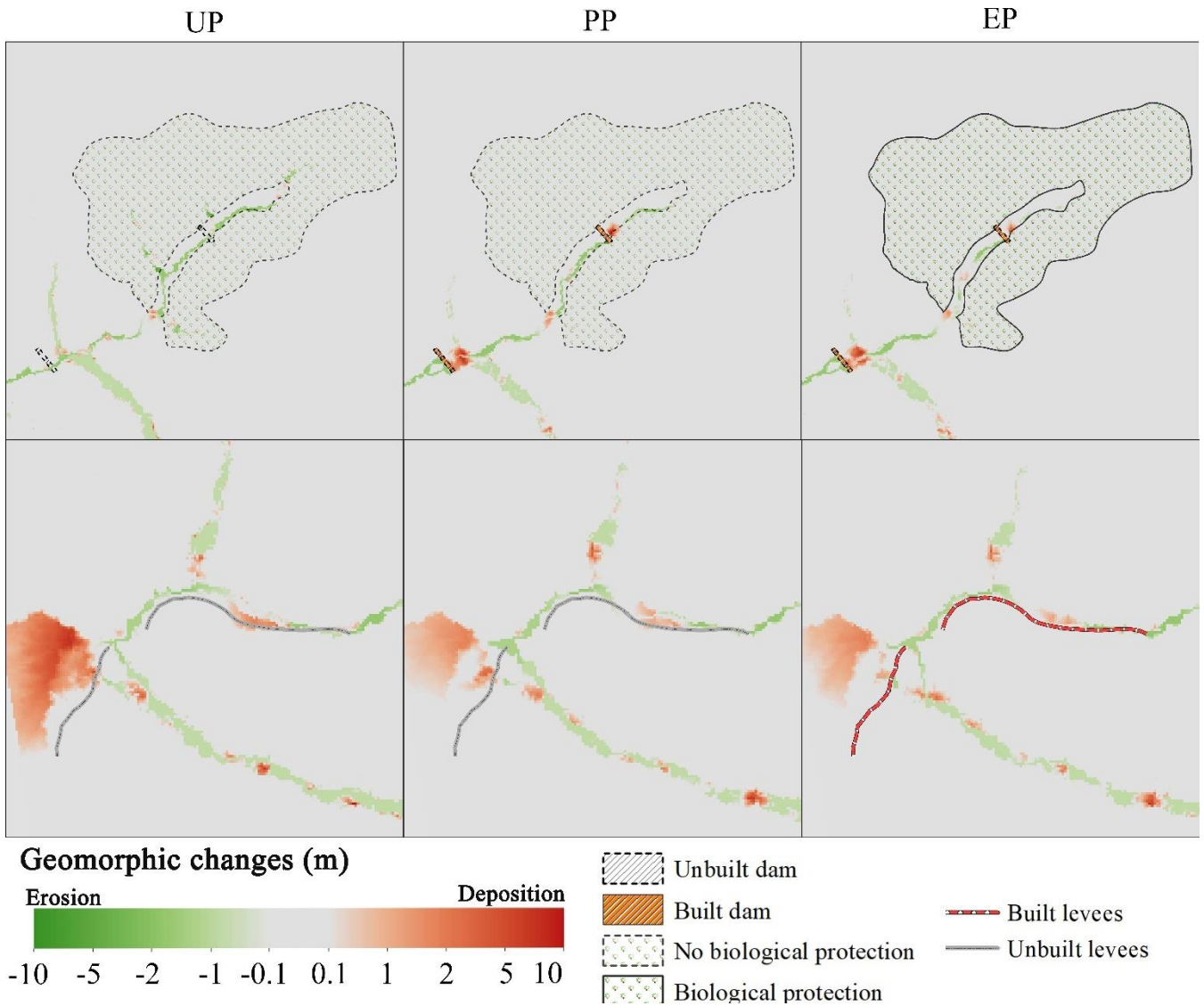
328

329

As shown in Fig. 7, the controlling measures and surroundings for the three scenarios were further investigated. Behind the two dams upriver in Scenarios PP and EP, the evident orange clusters indicate that the deposition occurred in Scenario PP and EP. In contrast, these locations were dominated by erosion, shown in green in scenario UP. Further analysis of the sediment depth shown in Figure 8 showed that the deposited depth behind the dams in Scenario EP was lower than that in Scenario PP. Additionally, in Scenario PP, sediment trapped by dam 1 was less than that by dam 2, but both have deposit thicknesses of more than 10 m, which exceeded the dams' heights (dam 1's height is 10 m, dam 2's height is 9 m). As for the simulation results in Scenario EP, the values of deposition depth behind the two dams were nearly 8 m, which were lower than the dams' heights.

The additional biological protection measure alters the material produced from the upriver tributary gullies varied due to the additional biological protection measures in three scenarios. A sediment volume of $14.4 \times 10^4 \text{ m}^3$ sediments was transported from EP's biological protection area in the EP scenario (solid lines in Fig. 7). A total of $27.1 \times 10^4 \text{ m}^3$ and $16.9 \times 10^4 \text{ m}^3$ of loose material were produced in the same region without biological protection in Scenarios UP

330 and PP, respectively. The vegetation revegetation enhanced the enhances sediment conservation based on the role of dam 1. -Com-
 331 pared with the deposition in UP and PP without levees in the downriver area (shown in the bottom row of Fig. 7), Fig. 7, the
 332 levees in EP blocked block debris in the bend of the channel and played play an essential role in protecting the residents and
 333 cultivated land behind the levees.
 334



335
 336 **Figure 7: Geomorphic changes at key spots/locations of the simulation results for the UP, PP, and EP scenarios. The top row is the**
 337 **upriver extent containing dam 1, dam 2 and the vegetation revegetation. The bottom row is the downriver extent containing levees.**

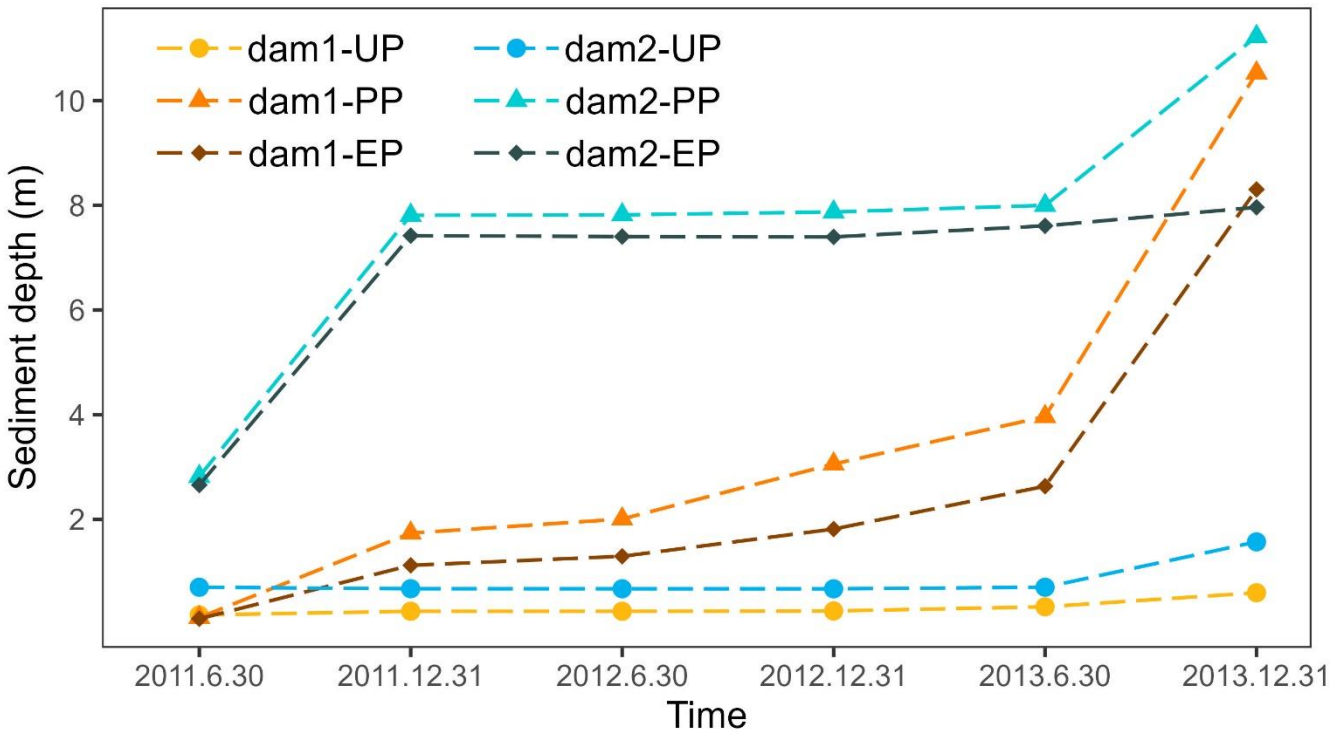
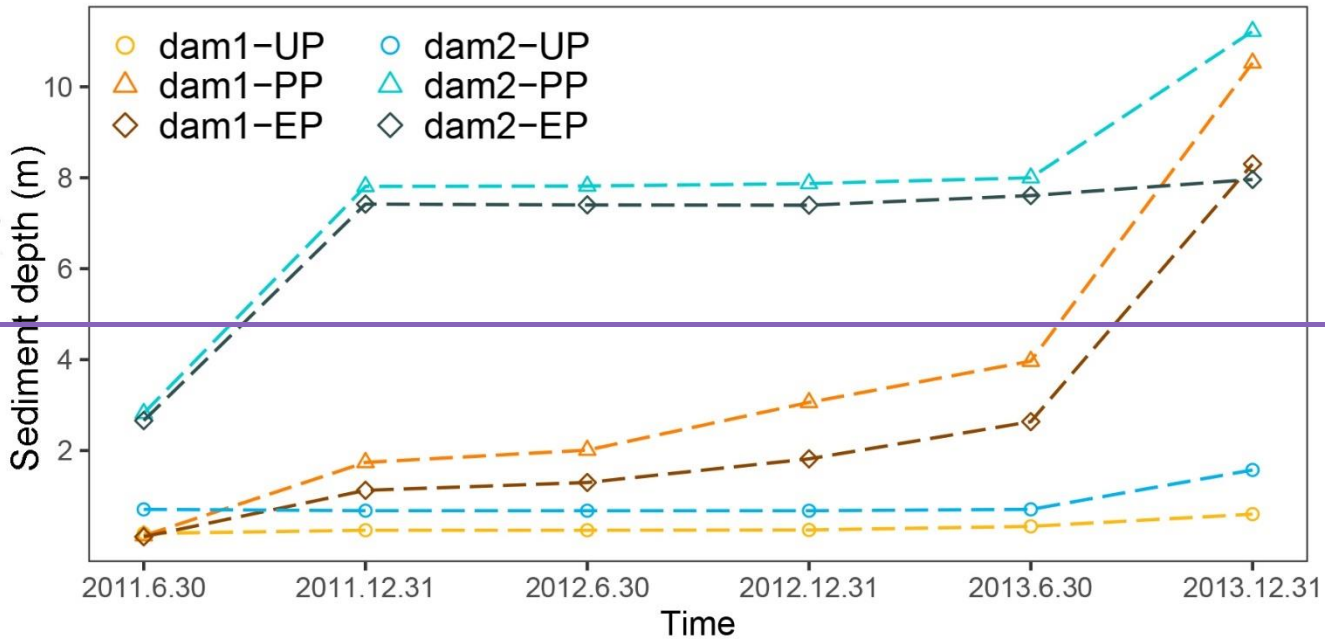
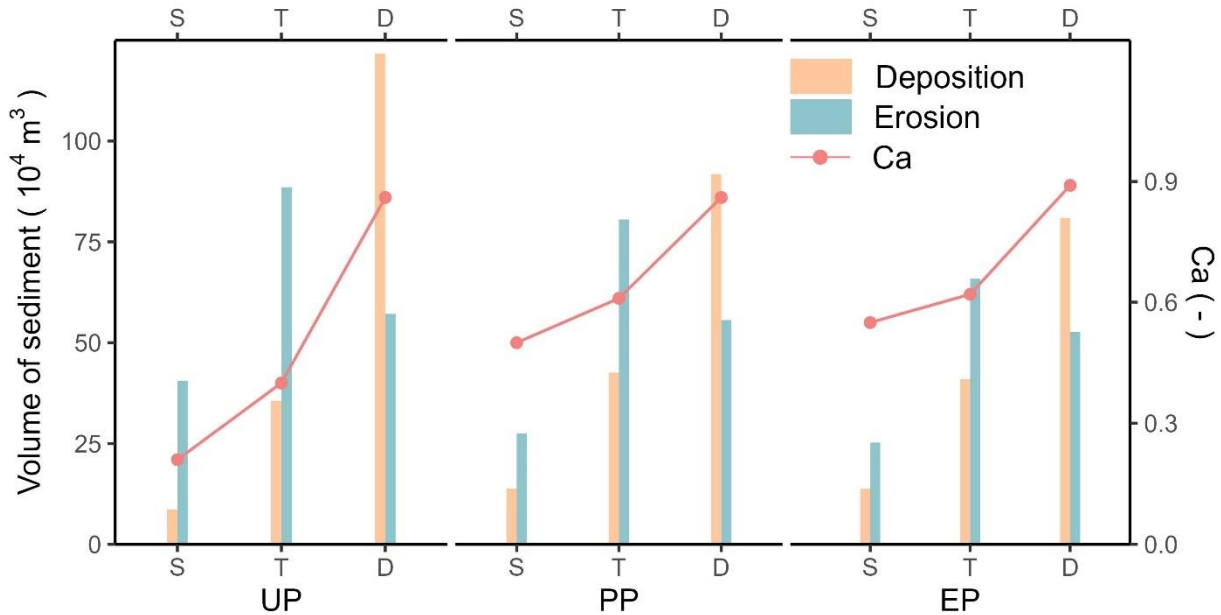


Figure 8: The depth of deposited sediment in the dams' placements.

4.4 Effectiveness assessment of the intervention measures

Figure 9 shows the erosion and deposition volumes in the source, transitional, and deposit areas and compares the conservation ability (Ca) in each scenario. For all three scenarios, the deposition volume in the source area was less than that in the transitional area, and the largest amount of sediment was deposited/accumulated in the deposit area. Regarding the eroded sediment, the largest volume was in the transitional area, followed by the transitional area, and the source area presents the lowest volume. Moreover, sediment transport was best controlled in the deposit area and worst contained in the source area under any intervention conditions.

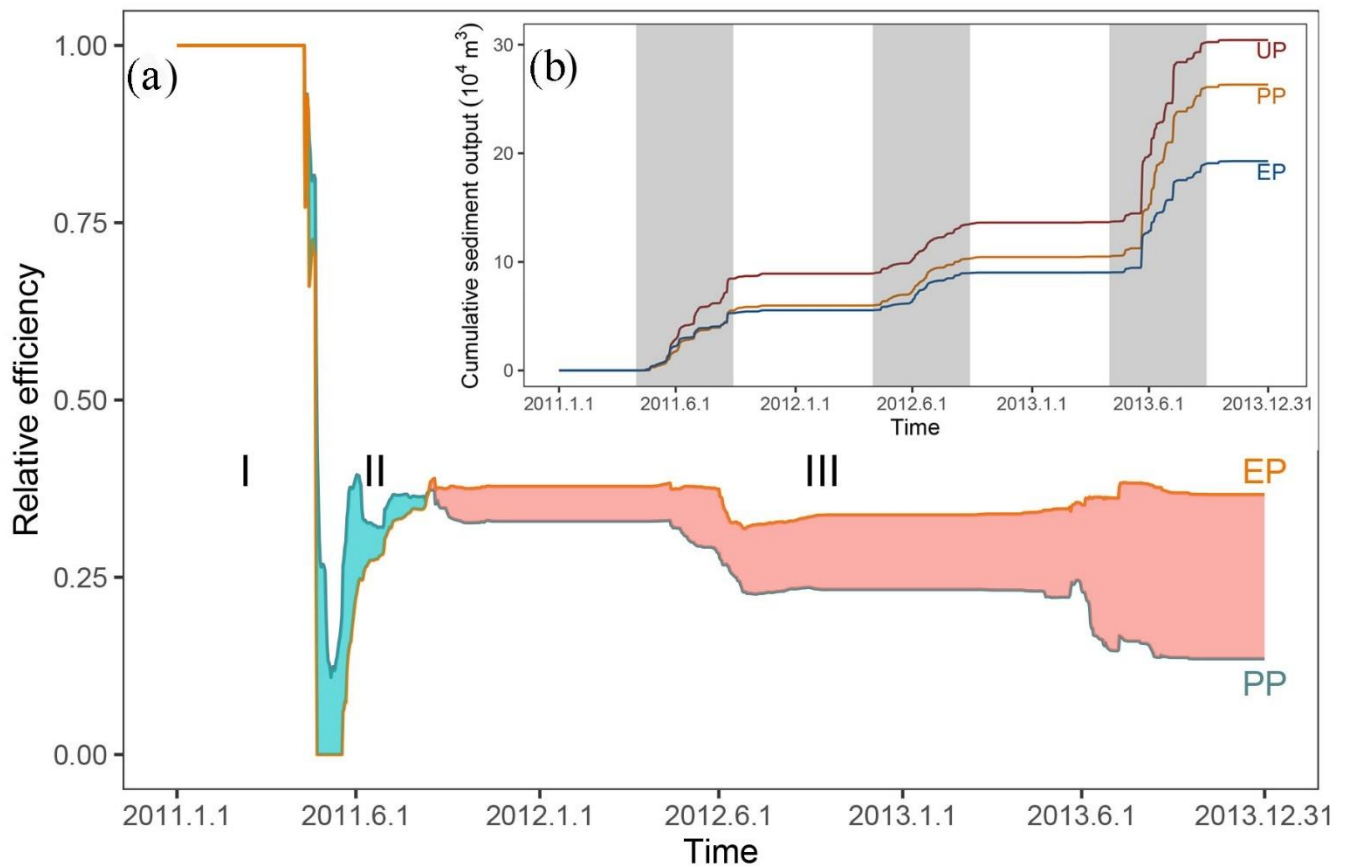
348 Compared with the Ca of the source area in Scenario UP, the value ~~was increased~~ increases by 138.1% in Scenario PP, which
 349 ~~was is~~ attributed to ~~the~~ dam1. Likewise, dam 2 in the transitional area ~~reduced~~ effectively reduces sediment loss ~~effectively~~,
 350 which ~~was is~~ reflected by a 52.5% increase in Ca . Furthermore, the mitigation measures in Scenario PP with vegetation re-
 351 tement and levees in Scenario EP ~~worked better~~ act best. The conservation ability in the source area increased by 161.9% due to
 352 the dam retainment and vegetation re-
 353 tement, and the levees helped increase the Ca by 3.49% in the deposit area.



354 **Figure 9: The volumes of sediment and the conservation ability (Ca) in the three areas for each scenario (S: source area; T: transi-
 355 tional area; D: deposit area).**

357 The cumulative sediment yield time series for each scenario and the relative efficiency of ~~scenarios~~ scenarios UP and EP are
 358 ~~present~~ presented in ~~Fig. 10b~~ Fig. 10b and ~~Fig. 10a~~ Fig. 10a, respectively. The steep curve of the output cumulative sediment
 359 ~~means~~ indicates a significant increase in the deposition. Three increasing stages are consistent with the rainfall intensity in the
 360 three monsoons (May-~~September~~ Sept). The total sediment output in UP ~~was is~~ the largest ~~of at~~ at $\sim 30.4 \times 10^4 m^3$; followed by the
 361 sediment yield ~~in of~~ of PP (at $26.3 \times 10^4 m^3$); and EP ~~presented~~ produced the least ~~figure~~ (material at $19.3 \times 10^4 m^3$).

362 The relative efficiency over the period of controlling measures by human intervention in PP and EP (~~Fig. 10b~~ Fig. 10a) indi-
 363 cates three distinct stages. Stage I shows that the intervention measures in both scenarios ~~prevented the~~ completely prevent
 364 sediment transport ~~completely~~. Later stage II ~~is~~ shows a peculiar period when the effect of enhanced protective measures in EP
 365 ~~was not as good as~~ as ~~pales in comparison with~~ that in PP through repeated experiments. For stage III, the relative efficiency of
 366 the intervention measures in EP ~~was is~~ greater than that in UP ~~for a more prolonged stage III~~, which ~~could achieve~~ achieves the
 367 long-term effect and stable conservation of solid material.



369

370

371

372

Figure 10: (a) cumulative sediment yield over time (grey region highlighting three monsoons), (b) relative efficiency of scenarios UP and EP compared with the UP (cyan shading represents when PP is more effective than EP and red shading represents the opposite); (b) Cumulative sediment yield over time (grey region highlighting three monsoons).

373

5. Discussion

374

5.1 Model calibration and uncertainty

375

376

377

378

379

380

381

382

383

384

385

386

387

388

389

The calibration and uncertainty are essential issues in the CAESAR-Lisflood (C-L) simulation of the geomorphic response to intervention measures based on the CA framework (Yeh and Li, 2006). A preliminary calibration was carried out by replicating reproducing the geomorphic changes and water depth driven by an extreme rainfall event that occurred in 2018. The results (Fig. S3) demonstrated that the C-L model successfully replicated the flash flood event using the initial conditions and model parameters. Actually, And the calibration of the replicating ability of the geomorphic response to the intervention measures was derived from a direct comparison between the model results and direct measurements (Fig. 4 (Fig. 4 and Fig. 5) Fig. 5). As a result, the simulated water discharge was more than the measured discharge but with the same order of magnitude. Moreover, the errors of erosion and deposition depth between the simulation in Scenario PP and photographic evidence at three locations were at most less than 20%. The results suggest the robustness of the model settings and parameterisation.

The source of uncertainty is mainly from the model parameters and driving factors. Skinner et al. (2018b) provided a detailed sensitivity analysis of C-L, indicating that the sediment transport formula significantly influences a smaller catchment modelled by 10 m-grid cells. The sediment transport law, and the Wilcock and Crowe equations (Wilcock et al., 2003) have been proven suitable in the Xingping valley (Xie et al., 2018, 2022a, b; Li et al., 2020). Nevertheless, the empirical models of sediment transport would overpredict bedload transport rates in steep streams (gradients greater than 3%) (D'Agostino and

390 Lenzi, 1999; Yager et al., 2012). Additionally, the driving factor, the input hourly rainfall data downscaled from the daily
391 sequence, is an unrealistic situation. Various sediment transport equations and downscaled hourly rainfall data need to be tested
392 in the C-L model to determine the further decrease uncertainty further.

393 **5.2 Intervention-The intervention effects**

394 ~~The~~ In this study, more facilities equivalent to create more comprehensive intervention systems ~~in this study which~~ aim to
395 control sediment delivery. The C-L simulation of model simulated the geomorphic responses to intervention measures
396 suggests and suggested the considerable influence of intervention measures on spatial modification and sediment
397 yield. The relative systematic intervention measures lead to fewer total affected areas (7.9%-19.7%) and lower sediment yieldy-
398 ields (16.7%-36.7%), which are suggested in the overall evidence (see Fig. 6 and Fig. 10). ~~Such~~ Fig. 6 and Fig. 10. The
399 model's prediction of the overall catchment-scale performance disturbed by the dynamics due to extreme event events is in line
400 with the viewpoints of other authors (Chen et al., 2023; Lan et al., 2020; Chen et al., 2015).

401 The mitigation measures considerably changed change the soil conservation ability in the three sub-regions, espe-
402 cially in the source area. ~~Herein, We hypothesise that the~~ two main reasons why for the decreased erosion material is less in the
403 source area than in another compared to the other two sub-regions are subregions can be inferred from the interactions of loose
404 material and topographic constraints. First, the abundant loose solid material formed by the strong earthquake have has stabi-
405 lised overall since ~~2008's~~ the 2008 debris flow (details in Table S1). Second, the long and deep gullies are mainly located in the
406 transitional area (Yaogouli, Shicouzi, Yangjiashan) and deposit area (Qingganging), which provide more sediment supply
407 than the source area. As shown in Fig. S4, the movement of the material occurred occurs mainly in the branch valleys in the
408 transitional and deposit area zones.

409 Moreover, comparing morphological details and the conservation ability with of the three scenarios stressed show the unique
410 role played by different intervention measures. For example, ~~the~~ check dams are most effective in blocking sediment, and ~~the~~
411 vegetation revetments strengthen the conservation ability. The synergysynergetic effect of the soil conservation ability of
412 checks increases by more than two-fold due to the combination of the check dams and vegetable the vegetation coverage is
413 created with an increase of more than two times. The levees are barriers with a discernable impact on sediment conservation
414 but with a special specific object-oriented protection.

415 The effectiveness of mitigation measures detected will decrease decreases over time with a smaller downward trend. We sup-
416 plement supplemented a ten-year experiment to reveal the decreasing declining trend over a more an extended period. We ran-
417 domly selected one of the 50 repeated rainfall datasets (year 2016-year 2025) downscaled by Li et al., 2020, which were
418 generated from the NEX-GDDP product (spatial resolution: 0.25°×0.25°, temporal resolution: daily) under the RCP 4.5 emis-
419 sion scenario. The extracted rainfall sequence was then input to into the C-L model to simulate the effectiveness of the three
420 intervention scenarios. The result (~~Fig. 11~~) (Fig. 11) illustrates that stage III (the stable stage that started on the 161st day, in
421 which Scenario EP's intervention measures were more effective) lasted longer than stages I and II, which were only at the start.
422 The relative effectiveness in both the PP and EP scenarios decreased gradually, while the curve fell faster in ~~PP~~ the PP scenario
423 (slope: -1.65×10^{-5}) than in the EP scenario (slope: -1.31×10^{-5}).

424 The storage capacity of the checking dams fades as with the accumulation of sediment deposits accumulated, which necessarily
425 lead leads to the a gradual decrease of in intervention effectiveness. Additionally, ~~the~~ vegetation revetments remain operationally
426 effective in reducing sediment transport by stabilising topsoil over the period when the role of dam reservoirs gradually fails
427 due to the lack of dredging work. Therefore, the vegetation protection strategy is vital for “green development” to reduce
428 sediment loss but requires further efforts.

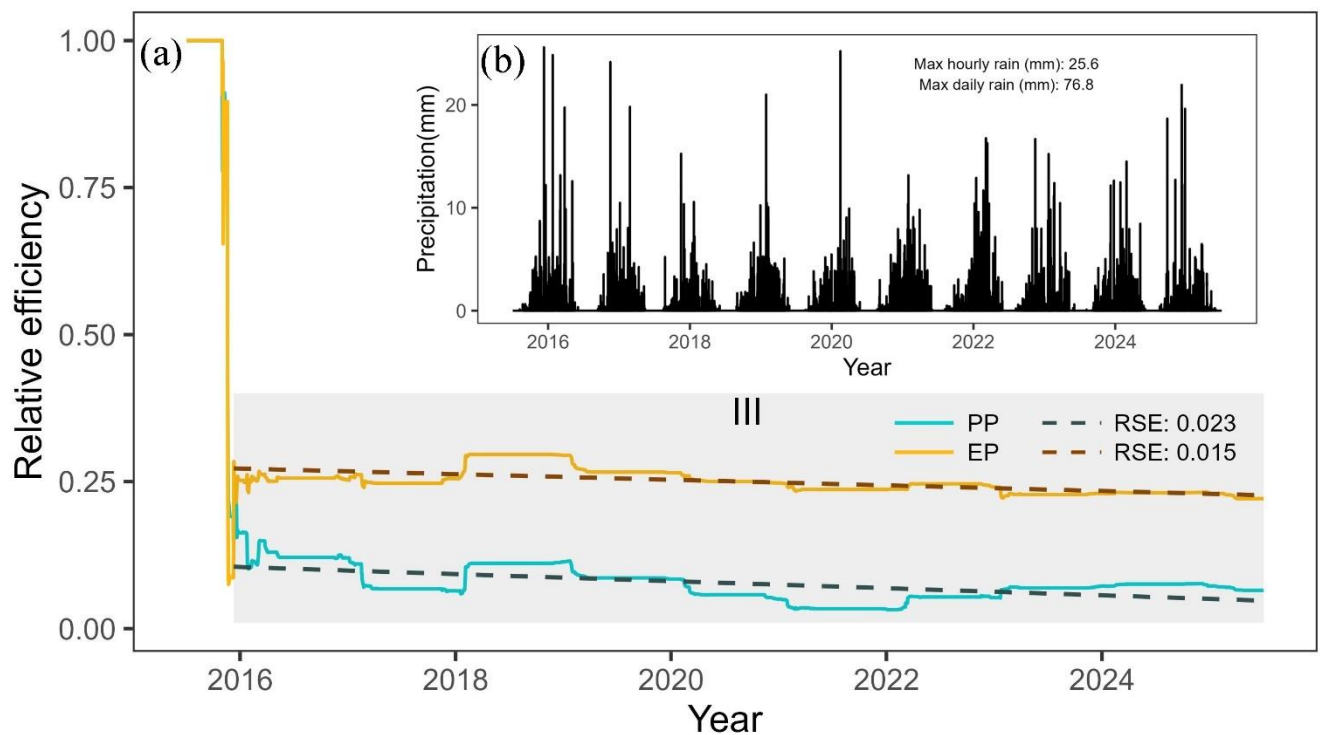
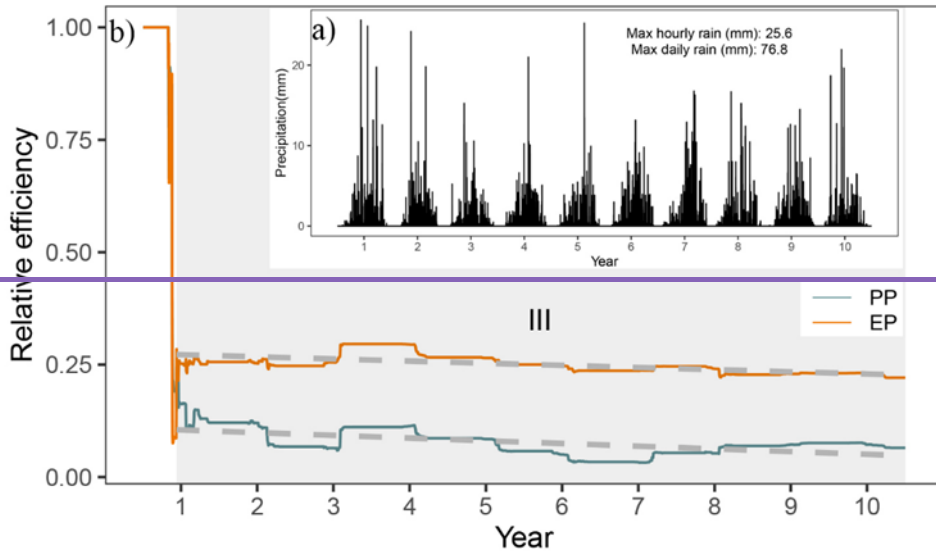


Figure 11: Future rainfall input of ten years and relative efficiency of sediment intervention measures. (a) rainfall downscaled from stochastic future rain; (b) the relative efficiency changes over ten years (the grey region highlighting stage III, and the grey dashed lines indicating the linear fitting curves); (b) Rainfall downscaled from NEX-GDDP (NASA Earth Exchange Global Daily Downscaled Projections) product.

5.23 Limitations and applications

We built the dams and levees in our simulations by increasing the elevation in the expected location and assuming that it could not be eroded (see <https://sourceforge.net/projects/caesar-lisflood/>). This method proved experimentally feasible (Poeppl et al., 2019; Gioia and Schiattarella, 2020). The rigid dam and levee body embedded in the model would not be broken or weakened over time so that the simulation result could underestimate the geohazard risk. Considering the complexity of the geo-hazard mechanism, the abovementioned tools could not simulate the occurrence process of geo-hazard chain links. They would ignore the fierce attack on possible instantaneous damage to the environment and facilities downstream. Some typical geo-hazard chains were have focused on the specified events in the short term and recreated the hazard lifecycle using physical and mechanical models (Fan et al., 2020).

444 The methods applied in the study further demonstrate that ~~the~~ C-L ~~model~~ is an effective tool for understanding ~~the~~ short- ~~to~~
445 medium-term or long-term ~~geomorphology~~~~geomorphological~~ changes (Ramirez et al., 2022; Li et al., 2020; Coulthard et al.,
446 2012a) and observing the effectiveness of natural hazard ~~interventions~~~~intervention~~ measures under different rainfall patterns.
447 Our simulations indicate that the mitigation facilities in this study ~~were~~~~are~~ effective, especially engineering efforts ~~cooperating~~
448 ~~with~~~~incorporating~~ vegetation revetments in the upstream area, which would help decision-makers ~~to~~ optimise the management
449 strategies to control mountain disasters. Geotechnical engineering has disadvantages, even though it is a mature technology
450 that identifies and fixes problems quickly (Cui and Lin, 2013), such as the ~~greater work~~~~need for extensive labour~~ and expense
451 and the difficulty of maintenance. While ~~the~~ “green development”, the ~~planting and maintenance of~~ vegetation cover ~~was~~
452 ~~effective in preventing~~~~can effectively prevent~~ erosion by strengthening topsoil and absorbing excess rainwater ~~with its~~~~via~~ roots
453 (Reichenbach et al., 2014; Stokes et al., 2014; Forbes and Broadhead, 2013; Mickovski et al., 2007). Alternatively, ~~the~~~~these~~
454 methods ~~could~~~~can~~ be used to study ~~the~~ tree planting patterns on different slopes.

455 6. Conclusions

456 In this study, ~~the~~ scenarios ~~intervented by~~~~involving~~ check dams, biological measures and artificial barriers ~~are~~~~were~~ simulated
457 using the C-L ~~model~~ to outline the erosion and deposition area, measure the impacts of blocking sediment, and examine how
458 ~~the vegetable~~~~vegetation~~ revetments ~~helped to~~~~help~~ stabilise ~~the slopes~~~~slopes~~. Four key findings are concluded. First, the engi-
459 neering measures ~~is~~~~used for~~ controlling sediment transport are efficient, and the performance in protecting the fragile environ-
460 ment ~~would~~~~can~~ be improved ~~combined by~~~~combining these engineering efforts~~ with other intervention measures ~~like,~~ ~~such as~~
461 vegetation ~~revetment~~~~revetments~~ and artificial barriers. Second, the effectiveness of mitigation measures ~~would~~~~de-~~
462 ~~creased~~~~decreases~~ over time. Third, the characteristics of ~~the~~ sediment transport patterns ~~changed~~~~alter~~ considerably ~~caused of~~~~due~~
463 ~~to~~ the intervention measures. The stabilising sediment ability in the source area increased by 161.9% with the additional effect
464 of vegetation revetments. ~~At last~~~~Finally~~, the present intervention measures ~~are~~ ~~inadequate~~~~need to be revised~~ to reduce erosion
465 and should be combined with dredging work.

466 Declaration of interest statement

467 The authors declare that they have no known competing financial interests or personal relationships that could have appeared
468 to influence the work reported in this paper.

469 Author contribution

470 Di Wang: Conceptualisation, Methodology, Software, Writing-original draft preparation. Ming Wang Kai Liu and Jun Xie:
471 Supervision, Methodology, Writing- Reviewing and Editing, Validation.

472 Acknowledgements

473 This research was supported by the National Key Research and Development Plan (2017YFC1502902). The financial support
474 is highly appreciated. The authors would also like to thank Professor Tom Coulthard and his team for their excellent work on
475 the freely available C-L model (<https://sourceforge.net/projects/caesar-lisflood/>).
476

477 **Reference**

- 478 Bates, P. D., Horritt, M. S., and Fewtrell, T. J.: A simple inertial formulation of the shallow water equations for efficient
479 two-dimensional flood inundation modelling, *J. Hydrol.*, 387, 33–45, <https://doi.org/10.1016/j.jhydrol.2010.03.027>, 2010.
- 480 Batty, M. and Xie, Y.: Possible urban automata, *Environ. Plan. B Plan. Des.*, 24, 175–192, <https://doi.org/10.1068/b240175>,
481 1997.
- 482 Beven, K.: Linking parameters across scales: subgrid parameterizations and scale dependent hydrological models, *Hydrol.*
483 *Process.*, 9, 507–525, <https://doi.org/https://doi.org/10.1002/hyp.3360090504>, 1995.
- 484 Beven, K.: TOPMODEL: A critical, *Hydrol. Process.*, 11, 1069–1085, [https://doi.org/https://doi.org/10.1002/\(SICI\)1099-](https://doi.org/https://doi.org/10.1002/(SICI)1099-)
485 [1085\(199707\)11:9<1069::AID-HYP545>3.0.CO;2-O](https://doi.org/https://doi.org/10.1002/(SICI)1099-1085(199707)11:9<1069::AID-HYP545>3.0.CO;2-O), 1997.
- 486 Beven, K. J. and Kirkby, M. J.: A physically based, variable contributing area model of basin hydrology, *Hydrol. Sci. Bull.*,
487 24, 43–69, <https://doi.org/10.1080/02626667909491834>, 1979.
- 488 Chen, N., Zhou, H., Yang, L., Yang, L., and Lv, L.: Analysis of benefits of debris flow control projects in southwest
489 mountains areas of China, *J. Chengdu Univ. Technol. (Science Technol. Ed.)*, 40, 50–58, <https://doi.org/10.3969/j.issn.1671->
490 [9727.2013.01.008](https://doi.org/10.3969/j.issn.1671-9727.2013.01.008), 2013.
- 491 Chen, X., Li, Z., Cui, P., and Liu, X.: Estimation of soil erosion caused by the 5.12 Wenchuan Earthquake, *J. Mt. Sci.*, 27,
492 122–127, 2009.
- 493 Chen, X., Cui, P., You, Y., Chen, J., and Li, D.: Engineering measures for debris flow hazard mitigation in the Wenchuan
494 earthquake area, *Eng. Geol.*, 194, 73–85, <https://doi.org/10.1016/j.enggeo.2014.10.002>, 2015.
- 495 Chen, Y., Li, J., Jiao, J., Wang, N., Bai, L., Chen, T., Zhao, C., Zhang, Z., Xu, Q., and Han, J.: Modeling the impacts of
496 fully-filled check dams on flood processes using CAESAR-lisflood model in the Shejiagou catchment of the Loess Plateau,
497 *J. Hydrol. Reg. Stud.*, 45, 101290, <https://doi.org/10.1016/j.ejrh.2022.101290>, 2023.
- 498 Cong, K., Li, R., and Bi, Y.: Benefit evaluation of debris flow control engineering based on the FLO-2D model, *Northwest.*
499 *Geol.*, 52, <https://doi.org/10.19751/j.cnki.61-1149/p.2019.03.019>, 2019.
- 500 Couclelis, H.: From cellular automata to urban models: new principles for model development and implementation, *Environ.*
501 *Plan. B Plan. Des.*, 24, 165–174, <https://doi.org/10.1068/b240165>, 1997.
- 502 Coulthard, T. J. and Skinner, C. J.: The sensitivity of landscape evolution models to spatial and temporal rainfall resolution,
503 *Earth Surf. Dyn.*, 4, 757–771, <https://doi.org/10.5194/esurf-4-757-2016>, 2016.
- 504 Coulthard, T. J. and Wiel, Van De J., M.: Modelling long term basin scale sediment connectivity, driven by spatial land use
505 changes, *Geomorphology*, 277, 265–281, <https://doi.org/10.1016/j.geomorph.2016.05.027>, 2017.
- 506 Coulthard, T. J., Macklin, M. G., and Kirkby, M. J.: A cellular model of Holocene upland river basin and alluvial fan
507 evolution, *Earth Surf. Process. Landforms*, 27, 269–288, <https://doi.org/10.1002/esp.318>, 2002.
- 508 Coulthard, T. J., Hancock, G. R., and Lowry, J. B. C.: Modelling soil erosion with a downscaled landscape evolution model,
509 *Earth Surf. Process. Landforms*, 37, 1046–1055, <https://doi.org/10.1002/esp.3226>, 2012a.
- 510 Coulthard, T. J., Ramirez, J., Fowler, H. J., and Glenis, V.: Using the UKCP09 probabilistic scenarios to model the amplified
511 impact of climate change on drainage basin sediment yield, *Hydrol. Earth Syst. Sci.*, 16, 4401–4416,
512 <https://doi.org/10.5194/hess-16-4401-2012>, 2012b.
- 513 Coulthard, T. J., Neal, J. C., Bates, P. D., Ramirez, J., de Almeida, G. A. M., and Hancock, G. R.: Integrating the
514 LISFLOOD-FP 2D hydrodynamic model with the CAESAR model: Implications for modelling landscape evolution, *Earth*
515 *Surf. Process. Landforms*, 38, 1897–1906, <https://doi.org/10.1002/esp.3478>, 2013.
- 516 Cui, P. and Lin, Y.: Debris-Flow Treatment: The Integration of Botanical and Geotechnical Methods, *J. Resour. Ecol.*, 4,
517 097–104, <https://doi.org/10.5814/j.issn.1674-764x.2013.02.001>, 2013.

518 Cui, P., Zhou, G. G. D., Zhu, X. H., and Zhang, J. Q.: Scale amplification of natural debris flows caused by cascading
519 landslide dam failures, *Geomorphology*, 182, 173–189, <https://doi.org/10.1016/j.geomorph.2012.11.009>, 2013.

520 D’Agostino, V. and Lenzi, M. A.: Bedload transport in the instrumented catchment of the Rio Cordon. Part II: Analysis of
521 the bedload rate, *Catena*, 36, 191–204, [https://doi.org/10.1016/S0341-8162\(99\)00017-X](https://doi.org/10.1016/S0341-8162(99)00017-X), 1999.

522 Einstein, H. A.: *The Bed-Load Function for Sediment Transportation in Open Channel Flows*, 1950.

523 Fan, X., Yang, F., Siva Subramanian, S., Xu, Q., Feng, Z., Mavrouli, O., Peng, M., Ouyang, C., Jansen, J. D., and Huang, R.:
524 Prediction of a multi-hazard chain by an integrated numerical simulation approach: the Baige landslide, Jinsha River, China,
525 *Landslides*, 17, 147–164, <https://doi.org/10.1007/s10346-019-01313-5>, 2020.

526 Feng, W., He, S., Liu, Z., Yi, X., and Bai, H.: Features of Debris Flows and Their Engineering Control Effects at Xinping
527 Gully of Pingwu County, *J. Eng. Geol.*, 25, <https://doi.org/10.13544/j.cnki.jeg.2017.03.027>, 2017.

528 Forbes, K. and Broadhead, J.: Forests and landslides: the role of trees and forests in the prevention of landslides and
529 rehabilitation of landslide-affected areas in Asia, *FAO*, 14–18 pp., 2013.

530 Gioia, D. and Schiattarella, M.: Modeling Short-Term Landscape Modification and Sedimentary Budget Induced by Dam
531 Removal: Insights from LEM Application, *Appl. Sci.*, 10, 7697, <https://doi.org/10.3390/app10217697>, 2020.

532 Goldberg, D. E.: *Genetic Algorithms in Search, Optimization, and Machine Learning*, Addison-Wesley Longman Publishing
533 Co., Inc., 372 pp., <https://doi.org/10.1007/BF01920603>, 1989.

534 Gorum, T., Fan, X., van Westen, C. J., Huang, R. Q., Xu, Q., Tang, C., and Wang, G.: Distribution pattern of earthquake-
535 induced landslides triggered by the 12 May 2008 Wenchuan earthquake, *Geomorphology*, 133, 152–167,
536 <https://doi.org/10.1016/j.geomorph.2010.12.030>, 2011.

537 Guo, Q., Xiao, J., and Guan, X.: The characteristics of debris flow activities and its optimal timing for the control in Shikan
538 River Basin Pingwu Country, *Chinese J. Geol. Hazard Control*, 29, <https://doi.org/10.16031/j.cnki.issn.1003-8035.2018.03.05>, 2018.

539 03. 05, 2018.

540 Hancock, G. R., Verdon-Kidd, D., and Lowry, J. B. C.: Soil erosion predictions from a landscape evolution model – An
541 assessment of a post-mining landform using spatial climate change analogues, *Sci. Total Environ.*, 601–602, 109–121,
542 <https://doi.org/10.1016/j.scitotenv.2017.04.038>, 2017.

543 He, J., Zhang, L., Fan, R., Zhou, S., Luo, H., and Peng, D.: Evaluating effectiveness of mitigation measures for large debris
544 flows in Wenchuan, China, *Landslides*, 19, 913–928, <https://doi.org/10.1007/s10346-021-01809-z>, 2022.

545 Huang, R.: *Geohazard assessment of the Wenchuan earthquake*, Science Press, Beijing, 944 pp., 2009.

546 Huang, R. and Fan, X.: The landslide story, *Nat. Geosci.*, 6, 325–326, <https://doi.org/10.1038/ngeo1806>, 2013.

547 J.B.C. Lowry, M. Narayan, G.R. Hancock, and K.G. Evans: Understanding post-mining landforms: Utilising pre-mine
548 geomorphology to improve rehabilitation outcomes, *Geomorphology*, 328, 93–107,
549 <https://doi.org/10.1016/j.geomorph.2018.11.027>, 2019.

550 Lan, H., Wang, D., He, S., Fang, Y., Chen, W., Zhao, P., and Qi, Y.: Experimental study on the effects of tree planting on
551 slope stability, *Landslides*, 17, 1021–1035, <https://doi.org/10.1007/s10346-020-01348-z>, 2020.

552 Lee, T. and Jeong, C.: Nonparametric statistical temporal downscaling of daily precipitation to hourly precipitation and
553 implications for climate change scenarios, *J. Hydrol.*, 510, 182–196, <https://doi.org/10.1016/j.jhydrol.2013.12.027>, 2014.

554 Li, C., Wang, M., and Liu, K.: A decadal evolution of landslides and debris flows after the Wenchuan earthquake,
555 *Geomorphology*, 323, 1–12, <https://doi.org/10.1016/j.geomorph.2018.09.010>, 2018.

556 Li, C., Wang, M., Liu, K., and Coulthard, T. J.: Landscape evolution of the Wenchuan earthquake-stricken area in response
557 to future climate change, *J. Hydrol.*, 590, 125244, <https://doi.org/10.1016/j.jhydrol.2020.125244>, 2020.

558 Marchi, L., Comiti, F., Crema, S., and Cavalli, M.: Channel control works and sediment connectivity in the European Alps,
559 *Sci. Total Environ.*, 668, 389–399, <https://doi.org/10.1016/j.scitotenv.2019.02.416>, 2019.

560 Mickovski, S. B., Bengough, A. G., Bransby, M. F., Davies, M. C. R., Hallett, P. D., and Sonnenberg, R.: Material stiffness,
561 branching pattern and soil matric potential affect the pullout resistance of model root systems, *Eur. J. Soil Sci.*, 58, 1471–
562 1481, <https://doi.org/10.1111/j.1365-2389.2007.00953.x>, 2007.

563 Poepl, R. E., Coulthard, T., Keesstra, S. D., and Keiler, M.: Modeling the impact of dam removal on channel evolution and
564 sediment delivery in a multiple dam setting, *Int. J. Sediment Res.*, 34, 537–549, <https://doi.org/10.1016/j.ijsrc.2019.06.001>,
565 2019.

566 Ramirez, J. A., Zischg, A. P., Schürmann, S., Zimmermann, M., Weingartner, R., Coulthard, T., and Keiler, M.: Modeling
567 the geomorphic response to early river engineering works using CAESAR-Lisflood, *Anthropocene*, 32,
568 <https://doi.org/10.1016/j.ancene.2020.100266>, 2020.

569 Ramirez, J. A., Mertin, M., Peleg, N., Horton, P., Skinner, C., Zimmermann, M., and Keiler, M.: Modelling the long-term
570 geomorphic response to check dam failures in an alpine channel with CAESAR-Lisflood, *Int. J. Sediment Res.*, 37, 687–700,
571 <https://doi.org/10.1016/j.ijsrc.2022.04.005>, 2022.

572 Reichenbach, P., Busca, C., Mondini, A. C., and Rossi, M.: The Influence of Land Use Change on Landslide Susceptibility
573 Zonation: The Briga Catchment Test Site (Messina, Italy), *Environ. Manage.*, 54, 1372–1384,
574 <https://doi.org/10.1007/s00267-014-0357-0>, 2014.

575 Saynor, M. J., Lowry, J. B. C., and Boyden, J. M.: Assessment of rip lines using CAESAR-Lisflood on a trial landform at the
576 Ranger Uranium Mine, *L. Degrad. Dev.*, 30, 504–514, <https://doi.org/10.1002/ldr.3242>, 2019.

577 Skinner, C. J., Coulthard, T. J., Schwanghart, W., Van De Wiel, M. J., and Hancock, G.: Global sensitivity analysis of
578 parameter uncertainty in landscape evolution models, *Geosci. Model Dev.*, 11, 4873–4888, <https://doi.org/10.5194/gmd-11-4873-2018>, 2018a.

579
580 Skinner, C. J., Coulthard, T. J., Schwanghart, W., Van De Wiel, M. J., and Hancock, G.: Global sensitivity analysis of
581 parameter uncertainty in landscape evolution models, *Geosci. Model Dev.*, 11, 4873–4888, <https://doi.org/10.5194/gmd-11-4873-2018>, 2018b.

582
583 Slingerland, N., Beier, N., and Wilson, G.: Stress testing geomorphic and traditional tailings dam designs for closure using a
584 landscape evolution model, in: *Proceedings of the 13th International Conference on Mine Closure*, 1533–1544,
585 https://doi.org/10.36487/ACG_rep/1915_120_Slingerland, 2019.

586 Stokes, A., Douglas, G. B., Fourcaud, T., Giadrossich, F., Gillies, C., Hubble, T., Kim, J. H., Loades, K. W., Mao, Z.,
587 McIvor, I. R., Mickovski, S. B., Mitchell, S., Osman, N., Phillips, C., Poesen, J., Polster, D., Preti, F., Raymond, P., Rey, F.,
588 Schwarz, M., and Walker, L. R.: Ecological mitigation of hillslope instability: Ten key issues facing researchers and
589 practitioners, *Plant Soil*, 377, 1–23, <https://doi.org/10.1007/s11104-014-2044-6>, 2014.

590 Thomson, H. and Chandler, L.: Tailings storage facility landform evolution modelling, in: *Proceedings of the 13th*
591 *International Conference on Mine Closure*, 385–396, https://doi.org/10.36487/ACG_rep/1915_31_Thomson, 2019.

592 Wang, M., Yang, W., Shi, P., Xu, C., and Liu, L.: Diagnosis of vegetation recovery in mountainous regions after the
593 wenchuan earthquake, *IEEE J. Sel. Top. Appl. Earth Obs. Remote Sens.*, 7, 3029–3037,
594 <https://doi.org/10.1109/JSTARS.2014.2327794>, 2014a.

595 Wang, M., Liu, M., Yang, S., and Shi, P.: Incorporating Triggering and Environmental Factors in the Analysis of
596 Earthquake-Induced Landslide Hazards, *Int. J. Disaster Risk Sci.*, 5, 125–135, <https://doi.org/10.1007/s13753-014-0020-7>,
597 2014b.

598 Wang, N., Han, B., Pang, Q., and Yu, Z.: post-evaluation model on effectiveness of debris flow control, *J. Eng. Geol.*, 23,
599 219–226, <https://doi.org/10.13544/j.cnki.jeg.2015.02.005>, 2015.

600 Van De Wiel, M. J., Coulthard, T. J., Macklin, M. G., and Lewin, J.: Embedding reach-scale fluvial dynamics within the
601 CAESAR cellular automaton landscape evolution model, *Geomorphology*, 90, 283–301,
602 <https://doi.org/10.1016/j.geomorph.2006.10.024>, 2007.

603 Wilcock, P. R., Asce, M., and Crowe, J. C.: Surface-based Transport Model for Mixed-Size Sediment Surface-based
604 Transport Model for Mixed-Size Sediment, 9429, [https://doi.org/10.1061/\(ASCE\)0733-9429\(2003\)129](https://doi.org/10.1061/(ASCE)0733-9429(2003)129), 2003.

605 Xie, J., Wang, M., Liu, K., and Coulthard, T. J.: Modeling sediment movement and channel response to rainfall variability
606 after a major earthquake, *Geomorphology*, 320, 18–32, <https://doi.org/10.1016/j.geomorph.2018.07.022>, 2018.

607 Xie, J., Coulthard, T. J., and McLelland, S. J.: Modelling the impact of seismic triggered landslide location on basin
608 sediment yield, dynamics and connectivity, *Geomorphology*, 398, 108029, <https://doi.org/10.1016/j.geomorph.2021.108029>,
609 2022a.

610 Xie, J., Coulthard, T. J., Wang, M., and Wu, J.: Tracing seismic landslide-derived sediment dynamics in response to climate
611 change, *Catena*, 217, 106495, <https://doi.org/10.1016/j.catena.2022.106495>, 2022b.

612 Xu, C., Xu, X., Yao, X., and Dai, F.: Three (nearly) complete inventories of landslides triggered by the May 12, 2008
613 Wenchuan Mw 7.9 earthquake of China and their spatial distribution statistical analysis, *Landslides*, 11, 441–461,
614 <https://doi.org/10.1007/s10346-013-0404-6>, 2014.

615 Yager, E. M., Turowski, J. M., Rickenman, D., and McArdeell, B. W.: Sediment supply, grain protrusion, and bedload
616 transport in mountain streams, *Geophys. Res. Lett.*, 39, 1–5, <https://doi.org/10.1029/2012GL051654>, 2012.

617 Yang, Z., Duan, X., Huang, J., Dong, Y., Zhang, X., Liu, J., and Yang, C.: Tracking long-term cascade check dam siltation:
618 implications for debris flow control and landslide stability, *Landslides*, 18, 3923–3935, <https://doi.org/10.1007/s10346-021-01755-w>, 2021.

620 Yeh, A. G. O. and Li, X.: Errors and uncertainties in urban cellular automata, *Comput. Environ. Urban Syst.*, 30, 10–28,
621 <https://doi.org/10.1016/j.compenvurbsys.2004.05.007>, 2006.

622 Yu, B., Yang, Y., Su, Y., Huang, W., and Wang, G.: Research on the giant debris flow hazards in Zhouqu County, Gansu
623 Province on August 7, 2010, *J. Eng. Geol.*, 18, 437–444, <https://doi.org/10.3969/j.issn.1004-9665.2010.04.001>, 2010.

624 Zhang, L. and Liang, K.: Research on economic benefit evaluation of the prevention and cure project for debris flow,
625 *Chinese J. Geol. Hazard Control*, 16, 48–53, <https://doi.org/10.3969/j.issn.1003-8035.2005.03.011>, 2005.

626 Zhang, X., Wang, M., Liu, K., Xie, J., and Xu, H.: Using NDVI time series to diagnose vegetation recovery after major
627 earthquake based on dynamic time warping and lower bound distance, *Ecol. Indic.*, 94, 52–61,
628 <https://doi.org/10.1016/j.ecolind.2018.06.026>, 2018.

629 Zhou, H., Chen, N., Lu, Y., and Li, B.: Control Effectiveness of Check Dams in Debris Flow Gully: A Case of Huashiban
630 Gully in Earthquake Worst-stricken Area, Beichuan County, *J. Mt. Sci.*, 30, 347–354, <https://doi.org/10.3969/j.issn.1008-2786.2012.03.015>, 2012.

632